analytical chemistry

Article

pubs.acs.org/ac

Breath Analysis with Broadly Tunable Quantum Cascade Lasers

Katharina Wörle,[†] Felicia Seichter,[†] Andreas Wilk,[†] Chris Armacost,[‡] Tim Day,[‡] Matthias Godejohann,[§] Ulrich Wachter,[∥] Josef Vogt,[∥] Peter Radermacher,[∥] and Boris Mizaikoff*[,†]

[†]Institute of Analytical and Bioanalytical Chemistry, University of Ulm, 89081 Ulm, Germany

[‡]Daylight Solutions Inc., San Diego, California 92128, United States

[§]MG Optical Solutions GmbH, 86922 Eresing, Germany

[∥]Klinik für Anästhesiologie, Sektion Anästhesiologische Pathophysiologie und Verfahrensentwicklung, Universitätsklinikum Ulm, 89081 Ulm, Germany

Supporting Information

ABSTRACT: With the availability of broadly tunable external cavity quantum cascade lasers (EC-QCLs), particularly bright mid-infrared (MIR; 3−20 μm) light sources are available offering high spectral brightness along with an analytically relevant spectral tuning range of >2 μm. Accurate isotope ratio determination of $^{12}CO_2$ and $^{13}CO_2$ in exhaled breath is of critical importance in the field of breath analysis, which may be addressed via measurements in the MIR spectral regime. Here, we combine for the first time an EC-QCL tunable across the $^{12}CO_2/^{13}CO_2$ spectral band with a miniaturized hollow waveguide gas cell for quantitatively determining the $^{12}CO_2/^{13}CO_2$ ratio within the exhaled breath of mice. Due to partially overlapping spectral features, these studies are augmented by appropriate multivariate data evaluation and calibration techniques based on partial least-squares regression along with optimized data preprocessing. Highly accurate determinations of the isotope ratio within breath samples collected from a mouse intensive care unit validated via hyphenated gas chromatography−mass spectrometry confirm the viability of IR-HWG-EC-QCL sensing techniques for isotope-selective exhaled breath analysis.

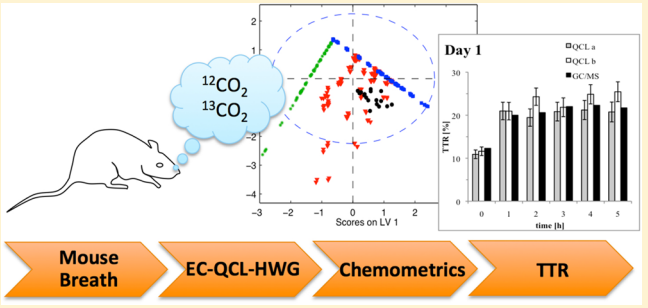

Quantum cascade lasers (QCLs) have seen a progressive development since their experimental introduction in 1994.[1−4] With the introduction of a broadly tunable external cavity quantum cascade laser providing tuning ranges up to 525 cm^{-1} across the MIR spectral band,[5] a wide variety of analytical applications may take advantage of such advanced light sources.[5−12] Recently developed EC-QCLs tuning across the ν_3-band of CO_2 (2125−2525 cm^{-1}) are of particular interest for application in medical diagnostics and exhaled breath analysis.

Carbon dioxide isotopologues are diagnostically relevant parameters for monitoring several disease patterns. For example, observing the isotope ratio of the CO_2 isotopologues $^{12}CO_2$ and $^{13}CO_2$ in exhaled breath samples is used for diagnosing Helicobacter pylori infection[13,14] or glucose metabolism dysfunction. The latter physiological condition is associated with septic shock, which is the most common cause of mortality in intensive care units in the United States.[15] During the state of sepsis or septic shock, the energy demand of a patient strongly increases, which results in hyperglycaemia[16] characterized, for example, by an enhanced consumption of peripheral glucose or *de novo* glucose synthesis.[17] Metabolization of glucose is a sensitive cycle, which is immediately affected by increasing blood glucose levels during hyperglycaemia. Consequently, the glucose cycle regulating the conversion of glucose and glucose-6-phosphate shifts toward an increase of glucose-6-phosphate, which in turn inhibits glycogenolysis.[18] As a result, the oxidation of glucose to CO_2 within skeletal muscles is inhibited by switching from carbohydrate to noncarbohydrate utilization.[19] Hence, noninvasively monitoring the glucose metabolism, for example, via exhaled breath biomarkers enables patient-specific medical care and early detection of sepsis and septic shock, respectively.

The present study takes advantage of the fact that both CO_2 isotopologues, $^{12}CO_2$ and $^{13}CO_2$, will be metabolized by the Krebs cycle. Hence, changes in the isotope ratio of exhaled carbon dioxide or metabolic intermediates such as alanine or lactate, for example, may directly be attributed to pathological metabolization processes. In order to detect a glucose metabolism dysfunction, ^{13}C-enriched glucose was administered during the studies presented herein, which is partially metabolized, and finally exhaled as $^{13}CO_2$. Consequently, changes of the so-called tracer-to-tracee ratio (TTR) (eq 1) in exhaled breath provide the first indications of a metabolic dysfunction.

Received: October 22, 2012
Accepted: January 15, 2013
Published: January 15, 2013

   dx.doi.org/10.1021/ac3030703 | *Anal. Chem.* 2013, 85, 2697−2702

$$\mathrm{TTR}(\%) = \left(\frac{c\ (\text{labeled tracer})}{c\ (\text{unlabeled tracee})}\right)100 \quad (1)$$

$$\delta^{13}C‰ = 1000\left(\frac{\frac{^{13}CO_2}{^{12}CO_{2(\text{sample})}} - \frac{^{13}CO_2}{^{12}CO_{2(\text{standard})}}}{\frac{^{13}CO_2}{^{12}CO_{2(\text{standard})}}}\right) \quad (2)$$

In medical studies, besides the TTR the so-called delta notation is common practice (eq 2). The δ value describes the isotopic abundance via a relative difference between the isotope ratio of a sample and a standard (i.e., most commonly the Vienna Pee Dee Belemnite[20] in units of marked isotope per mill ($\delta^{13}C‰$).

The determination of the CO_2 TTR may be realized by several analytical methods. The most commonly applied techniques involve isotope-selective mass spectrometry frequently combined with gas chromatography (GC-MS)[21−23] and isotope ratio mass spectrometry (IRMS).[21,23] Both methods provide exquisite sensitivity and selectivity with IRMS representing the gold standard for low ^{13}C enrichment levels in breath samples providing a linear response for samples up to a maximum enrichment of 924 $\delta^{13}C‰$.[24] GC-MS appears more suitable for higher enrichment levels of >60000 $\delta^{13}C‰$, which is the range relevant for exhaled mouse breath samples resulting from the very low lung volume and body mass of mice. Furthermore, the determination of several volatile breath constituents is enabled by GC-MS. However, instrumental dimensions and sampling prerequisites do not facilitate continuous online measurements next to the patient or animal. Hence, analyzing the isotope ratio via spectroscopic or sensing techniques may supplement current exhaled breath analysis methods with online monitoring capabilities and, upon appropriate miniaturization, determination in minute sample volumes, as required for mouse breath analysis.

Spectroscopic methods for the determination of CO_2 and its isotopologues are frequently taking advantage of the isotopic shift associated with IR absorption features resulting from their difference in molecular mass. The most commonly applied technology in clinical use is nondispersive isotope selective infrared spectroscopy (NDIRS).[25] NDIRS shows similar results as IRMS for enrichment levels of <800 $\delta^{13}C‰$ and provides less complex instrumentation. While revealing sufficient sensitivity and accuracy for most applications, NDIRS usually requires large sample volumes (500−1000 mL) and low oxygen content resulting in collisional line broadening. This requirement limits applicability in intensive care scenarios, as patients are frequently hyperoxic due to ventilation.[26]

Another alternative method in lieu of GC-MS measurements is laser-assisted ratio analysis (LARA),[27−29] which provides detection limits in the ppm range for isotope ratios; however, this method is also not suitable for online measurements.

Distributed feedback (DFB)-QCLs[30,31] are tunable semiconductor MIR lasers operating at room temperature and enabling temperature-controlled tuning of the emission wavelength in a narrow spectral window via a grating embedded at the surface of the active laser structure. Rubin et al.[32] used a DFB-QCL in the spectral region around 2300 cm^{-1} in a flow-through system for $^{12}CO_2/^{13}CO_2$ isotope ratio determination in human breath. The analysis is based on a Lorentzian fit of single rotational−vibrational lines for $^{12}CO_2$ and $^{13}CO_2$ within a spectral window of 2 cm^{-1} providing parts per billion (ppb) sensitivity for the determination of absolute $^{13}CO_2$ concentrations, which is important for detecting small changes of $\delta^{13}C‰$.

Combining QCLs with an external cavity and a movable grating nowadays offers a substantially enlarged tuning range compared to DFB-QCLs and facilitates evaluating broader absorption features in lieu of individual rotational−vibrational ones, thereby minimizing the effect of line-broadening processes during quantitative data evaluation. Hence, in the present study, a broadly tunable EC-QCL with a tuning range covering the ν_3 band of $^{12}CO_2$ and $^{13}CO_2$ with a single device was applied.

Aside from laser-based techniques, also Fourier transform-infrared spectroscopy (FT-IR) spectroscopic measurements are used for CO_2 isotopic ratio determinations. Hofstetter et al.[12] have shown a gas sensor prototype using an FT-IR spectrometer combined with a quantum cascade detector to exemplarily determine the $^{13}CO_2$ concentration in ambient air and human breath at ppb levels based on a comparison with simulated spectra.

The feasibility of determining the CO_2 TTR by combining FT-IR spectroscopy with a hollow core waveguide[33,34] (HWG) serving as both gas cell and light-propagating waveguide has recently been demonstrated by the research group of Mizaikoff.[35−37] The developed HWG gas cell enables FT-IR and EC-QCL experiments in particularly small sample volumes (i.e., approximately 100 μL providing an optimized signal-to-noise ratio). While the utility of FT-IR-HWG systems is undoubted, usage for mouse intensive care units and future bedside patient monitoring requires a substantially smaller device footprint, as demonstrated for the EC-QCL-HWG sensor system herein.

Due to the overlap within the ν_3 band of $^{12}CO_2$ and $^{13}CO_2$ spectra, multivariate data evaluation based on partial least-squares regression (PLS)[38] using the SIMPLS algorithm[39] was applied and the established calibration models were optimized for performance via appropriate data preprocessing routines.

Consequently, the aim of the present study was the quantitative determination of the CO_2 TTR in mouse breath samples using, for the first time, an EC-QCL-HWG gas sensor system along with validation of the results obtained via comparison to simultaneously recorded GC-MS data.

EXPERIMENTAL SECTION

IR measurements were performed using a broadly tunable pulsed EC-QCL (Daylight Solutions, San Diego, CA) as a light source combined with a miniaturized HWG gas cell. The gas cell comprises a 2.5 cm segment of silica Ag/AgI-coated HWG (outer Ø = 4.1 mm, inner Ø = 2.0 mm; Polymicro Technologies, Phoenix, AZ) embedded in a custom aluminum cube assembly and sealed with ZnSe windows (Macro Optica Ltd., Moscow, Russia). The cell assembly was designed for accommodating particularly small breath sample volumes (approximately 100 μL). Detection of IR radiation emanating at the distal end of the HWG was performed using a liquid nitrogen-cooled mercury−cadmium−telluride (MCT) detector (FT-IR 22-2.0, InfraRed Associates Inc., Stuart, FL). To avoid spectral interferences with ambient CO_2 and other air constituents, the entire optical setup was encased within an LDPE polymer bag (100 μ, dm Folien, Reutlingen, Germany), and was continuously purged with pure nitrogen (MTI IndustrieGase AG, Neu-Ulm, Germany).

As schematically shown in Figure 1, MIR radiation emitted by a broadly tunable EC-QCL (a) (model 11040-UT, Daylight

dx.doi.org/10.1021/ac3030703 | Anal. Chem. 2013, 85, 2697−2702

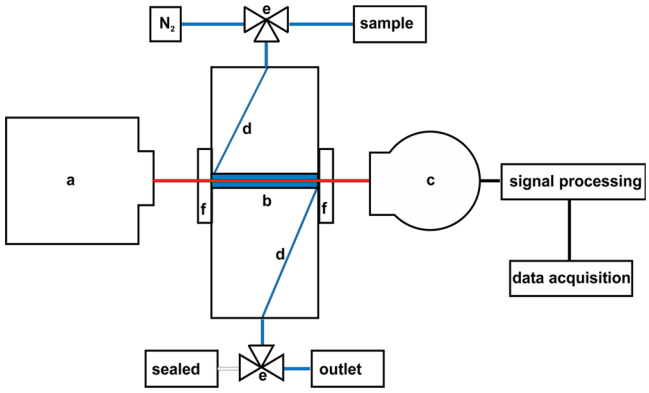

Figure 1. Schematic of the experimental setup for EC-QCL-HWG experiments; red: IR laser beam; blue: gas sample flow.

Solutions, San Diego, CA, USA) was directly coupled (proximity coupling) into the HWG assembly (b) and to the MCT detector (c) avoiding any coupling optics, thus providing a potentially compact sensor system. For mechanical and temperature stability, the HWG gas cell was embedded into an aluminum cube. The gas inlet capillary (d) was connected to a three-way valve (e), with one port sealed with a septum enabling injection of gas samples with minimum leakage. The third port of the valve was connected to a continuous N_2 flow. The gas outlet (d) was also connected to a three-way valve (e). The HWG used within this sensing module acts as both an IR radiation conduit and a compact sample cell. The HWG is sealed with MIR transparent ZnSe windows (f) (Macro Optica Ltd., Moscow, Russia). The amplified voltage signal from the detector was collected for each individual laser pulse via customized circuitry and processed after digitization using a notebook for data acquisition. The connection between the controller and the QCL was established via a GPIB/RS-232 interface. Laser tuning and data acquisition were controlled via a customized LabView module. The QCL operation parameters are summarized in Table 1.

Table 1. EC-QCL Operating Parameters

laser parameter	
operation mode	internal pulse
scan mode	manual step
laser current (mA)	1453
laser head temperature (°C)	15
duty cycle (%)	5
repetition frequency (kHz)	100
pulse width (displayed) (ns)	500
minimum wavenumber (cm^{-1})	2150
maximum wavenumber (cm^{-1})	2450
step size (cm^{-1})	0.5

Calibration samples of $^{13}CO_2$ and $^{12}CO_2$ were established via a gas mixing system (H. Wösthoff GmbH, Bochum, Germany) using a static mixing method based on induced turbulences between 50 mL syringes (B. Braun Melsungen AG, Melsungen, Germany).

For evaluating the ν_3 band of the CO_2 isotopes $^{12}CO_2$ (@ 2349 cm^{-1}) and $^{13}CO_2$ (@2283 cm^{-1}), the spectral region of 2150−2450 cm^{-1} was scanned with the EC-QCL at a step width of 0.5 cm^{-1}. For data evaluation, the target wavenumber was consistently applied (deviation from the measured wavenumber, 0.05 cm^{-1} max due to the wavelength uncertainty introduced by the pulsed laser).

Over a total analysis period of 5 h, each hour three breath samples were collected from an anaesthetized and ventilated mouse (one 3 mL sample and two 1 mL samples) via appropriate plastic syringes. The 3 mL sample was used for EC-QCL measurements studies, while the remaining samples were applied for validation by GC-MS analysis. For a comparison of GC-MS with EC-QCL-HWG, data over three individual measurement periods were collected.

Multivariate calibration and data evaluation were performed via Matlab (MATLAB 7.10.0.499 R2010a, The MathWorks Inc., Natick, MA) using the PLS Toolbox (PLS Toolbox 6.2.1, Eigenvector Research Inc., Wenatchee, WA). PLS models were calculated using a set of 367 calibration samples containing $^{12}CO_2$ in a range of 0.1−6.9%, $^{13}CO_2$ in a range of 0.05−3.0%, and synthetic ^{13}C-enriched gas samples bracketing 0.5 to 100% enrichment. Validation of the models was performed selecting nine test samples treated as quasi unknowns.

RESULTS AND DISCUSSION

For optimizing the multivariate data analysis strategy, spectral region selection was compared the utilizing the entire spectral range.

Evaluation of the Entire ν_3 Band. PLS regression was applied using the SIMPLS algorithm[39] based on three latent variables (LVs) capturing 99.24% of the spectral variance and 98.01% of the variance in calibration after singular value decomposition (SVD). In contrast to previously published PLS models based on FT-IR-HWG studies, EC-QCL-HWG experiments apparently require a third latent variable, which may account for signal fluctuations due to wavelength uncertainties introduced by frequency shifts during individual laser pulses.[37] After optimization, smallest predictive errors were achieved by applying the following data preprocessing steps on the raw x data (spectra covering a spectral range of 2201−2415.5 cm^{-1}) in sequence: (i) standard normal variate scaling (SNV) with an offset of 0.5, (ii) baseline correction within the range of 2201−2208 and 2406.5−2414 cm^{-1}, (iii) smoothing with a Savitzky-Golay algorithm and a filter size of 3 pt, and (iv) group scaling with two blocks. The y data (i.e., the related concentration values) were preprocessed by autoscaling.

The combination of these data preprocessing steps led to a calibration model with coefficients of determination (COD) for $^{12}CO_2$ and $^{13}CO_2$ of 0.979 and 0.983 with a root-mean-square error of calibration (RMSEC) of 0.190 and 0.077 for $^{12}CO_2$ and $^{13}CO_2$, respectively. Selecting different quasi unknowns, and thus calibration samples, improved the COD but not the predictive capability of the model. This is represented by the root-mean-square error of prediction (RMSEP), which amounts to 0.215 for $^{12}CO_2$ and 0.116 for $^{13}CO_2$. Figure 2 shows the resulting calibration function.

Comparing the ideal correlation function (Figure 2, green line) and the calculated fit (Figure 2, red line) reveals a minute nonlinearity for $^{13}CO_2$ at concentrations of >1%. This phenomenon was already observed during previous studies using an FT-IR-HWG system and is subject to detailed ongoing research for quantifying and potentially correcting these effects.[37]

In Figure 3, a scores plot of the three latent variables illustrates their interrelation. $^{12}CO_2$ and $^{13}CO_2$ show an inverse behavior within the data space spanned by the three LVs. The

dx.doi.org/10.1021/ac3030703 | Anal. Chem. 2013, 85, 2697−2702

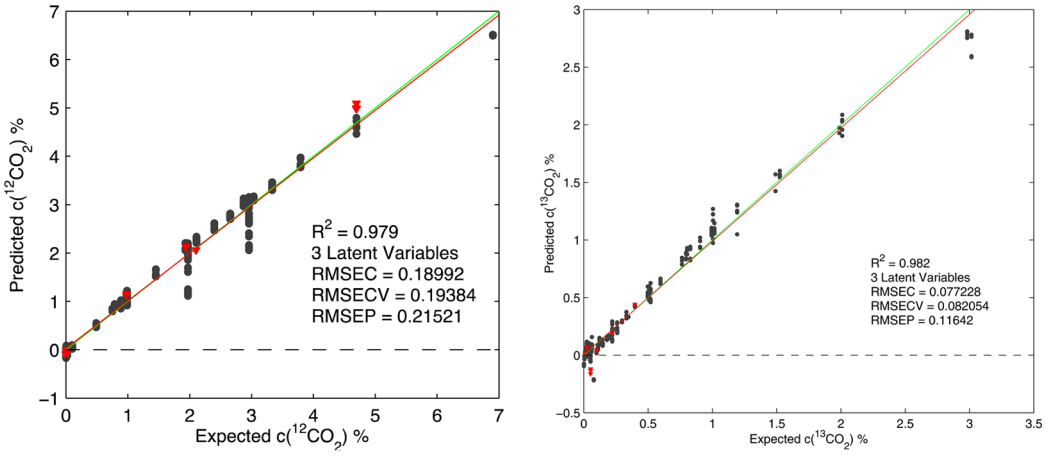

Figure 2. Expected vs predicted CO_2 concentration, (left) $^{12}CO_2$ and (right) $^{13}CO_2$. Dots represent calibration samples and triangles test samples (quasi unknowns). Red line: linear fit and green line: $y = x$.

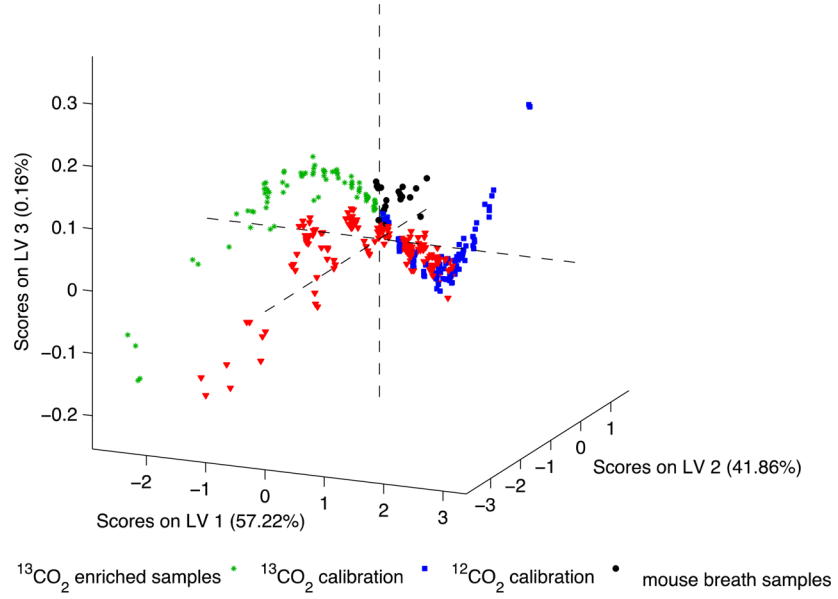

Figure 3. Scores plot illustrating the interrelation of the analyzed data within the three latent variables.

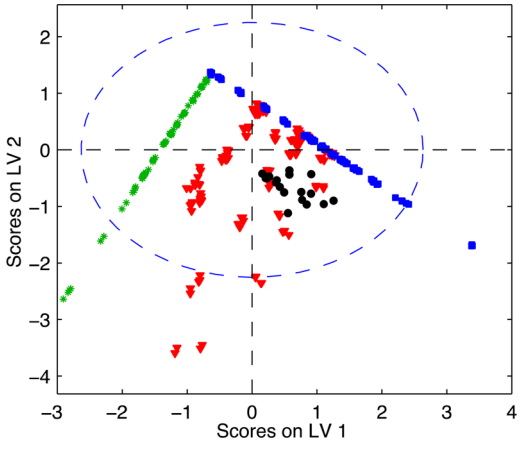

Figure 4. Radar plot of the scores of LV1 vs LV2. Black: mouse breath samples, green: $^{13}CO_2$ calibration samples, blue: $^{12}CO_2$, and red: $^{13}CO_2$-enriched samples.

^{13}C-enriched samples are located between the two branches of nonenriched samples and show a similar trend according to the

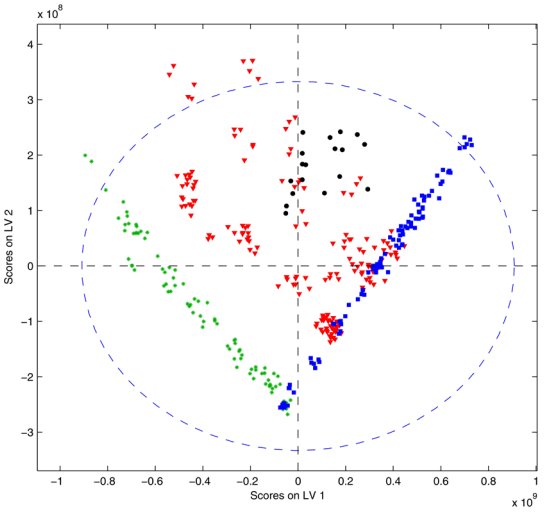

Figure 5. Radar plot of the scores of LV1 vs LV2. Black: mouse breath samples, green: $^{13}CO_2$ calibration samples, blue: $^{12}CO_2$, and red: $^{13}CO_2$ enriched samples.

dx.doi.org/10.1021/ac3030703 | *Anal. Chem.* 2013, 85, 2697−2702

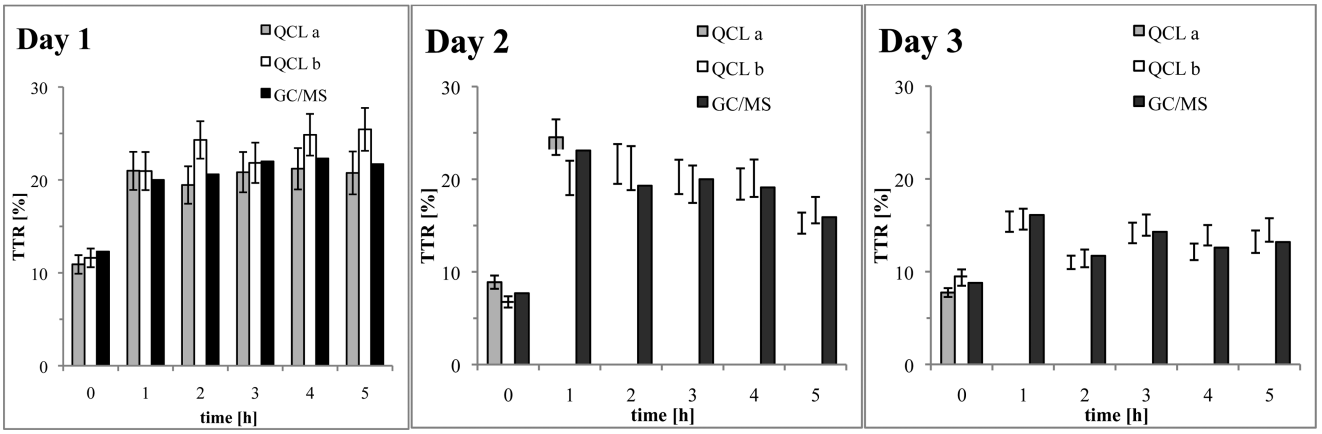

Figure 6. Summary of the obtained results for mouse breath samples independently analyzed on three different days: Gray, results EC-QCL-HWG data evaluated using the entire spectral range (QCL a); white, results EC-QCL-HWG data evaluated using spectral region selection (QCL b); and black, GC-MS data.

grade of enrichment. The analyzed 18 mouse breath samples are likewise distributed in the regime of the ^{13}C-enriched samples at the center of the model, yet, might be related to higher neat CO_2 concentrations rather than enriched calibration samples.

Taking only the first two latent variables into account, a radar plot (figure 4) illustrates the analyzed mouse breath samples within a 95% confidence level. Outside the confidence level, $^{13}CO_2$ and $^{13}CO_2$-enriched samples with a $^{13}CO_2$ content of >1.5% and $^{12}CO_2$ > 5% are located. Including these samples improves the resulting calibration model. The enriched samples are located parallel to the $^{13}CO_2$ branch and are linked to the basic $^{12}CO_2$ concentration.

The resulting model was applied to determine the concentration of $^{13}CO_2$ and $^{12}CO_2$ within 18 collected mouse breath samples represented as the tracer-to-tracee ratio (TTR). For validation, samples of the same breath batch were analyzed via GC-MS; the obtained results are summarized in Figure 6. For these data and the developed data evaluation methodology, a mean relative deviation of −1.1% (absolute deviation: 5.8%) between the EC-QCL-HWG and GC-MS data was achieved, thereby corroborating excellent agreement between the EC-QCL-HWG and GC-MS validation measurements.

Evaluation after Spectral Region Selection. Due to the overlap of the ν_3 bands of $^{12}CO_2$ and $^{13}CO_2$, an alternative approach for data evaluation after spectral region selection was investigated. For $^{13}CO_2$, the spectral range of 2249−2270 cm^{-1} and for $^{12}CO_2$, the spectral range of 2345−2360 cm^{-1} were selected. In general, slightly improved predictive capabilities were observed due to less perturbation by overlaying absorption bands of both isotopologues. Similar to the evaluation of the entire ν_3 band, a set of optimized data preprocessing methods was applied in following sequence: (i) baseline correction using weighted least-squares, (ii) standard normal variate scaling, (iii) mean centering, and (iv) poisson scaling. In contrast to previously applied group scaling, poisson scaling scales the data by a factor S, which represents the square root of the mean of the data.

Optimum results were achieved by reducing the considered concentration range to a maximum of 5% for $^{12}CO_2$ and 2% for $^{13}CO_2$, respectively. The resulting calibration model was also based on 3 LVs and captures a spectral variance of 97.71% and a calibration variance of 95.96%. The obtained CODs for this model are 0.961 for $^{13}CO_2$ and 0.959 for $^{12}CO_2$, respectively. Testing the predictability of the model offers a RMSEP of 0.256 for $^{12}CO_2$ and of 0.051 for $^{13}CO_2$. The RMSEC was determined at 0.242 for $^{12}CO_2$ and 0.088 for $^{13}CO_2$, respectively.

The obtained calibration functions are comparable to the ones obtained using the entire spectral range (see the Supporting Information); likewise, the analyzed mouse breath samples distribute well within the set of calibration samples, as shown in Figure 5.

Thus, obtained TTR of mouse breath samples along with the relative deviation to the GC-MS measurements are summarized in Figure 6. The obtained results reveal excellent agreement between the EC-QCL-HWG data and the GC-MS validation data. The mean relative deviation of the TTR determination is 3.4% (absolute mean deviation: 7.8%).

Figure 6 gives a summary overview of all calculated TTR values based on EC-QCL-HWG data, along with the related GC-MS validation data. As there is no evident trend in over- or underestimating the TTR, systematic errors may be excluded. The results based on an evaluation of the entire spectral range (QCL a) reveal a slightly better compliance with the validation data compared to the results obtained after spectral region selection (QCL b).

■ CONCLUSIONS

The present study for the first time demonstrates the feasibility to determine the TTR of CO_2 isotopologues (i.e., $^{12}CO_2$ and $^{13}CO_2$) in small volumes (few hundred microliters) of mouse breath samples via a novel sensor system combining an external cavity quantum cascade laser with a miniaturized mid-infrared hollow waveguide gas cell. Validation by GC-MS analysis revealed excellent agreement with the obtained IR data. Appropriate multivariate data evaluation strategies (PLS) along with optimized data preprocessing steps successfully compensated for wavelength fluctuations inherent in the pulsed EC-QCL used in this study. While evaluation of the entire spectral window (approximately 400 cm^{-1}) compared slightly better with the GC-MS validation data, spectral region selection offers substantially faster data acquisition rates, thereby rendering this newly developed IR sensing system ideally suited for future online monitoring of the TTR within mouse intensive care units. Finally, with the present study, EC-QCL-HWG sensing systems have clearly demonstrated their

dx.doi.org/10.1021/ac3030703 | Anal. Chem. 2013, 85, 2697−2702

potential as breath diagnostic devices, which may in the future be harnessed for direct online analysis of exhaled breath also in human intensive care analysis, therapy progression monitoring, or medication compliance testing.

■ ASSOCIATED CONTENT

Supporting Information

Additional information as noted in text. This material is available free of charge via the Internet at http://pubs.acs.org.

■ AUTHOR INFORMATION

Corresponding Author

*E-mail: boris.mizaikoff@uni-ulm.de.

Notes

The authors declare no competing financial interest.

■ ACKNOWLEDGMENTS

The authors acknowledge the support of the team operating the mouse intensive care unit (MICU) at the Klinik für Anästhesiologie, Sektion Anästhesiologische Pathophysiologie und Verfahrensentwicklung, Universitätsklinikum Ulm, and especially Sandra Weber for assistance during the mouse breath studies. The study protocol for mouse experiments was approved by the University Animal Care Committee and by the federal authorities for animal research of the Regierungspräsidium Tübingen, Baden-Württemberg, Germany.

■ DEDICATION

Dedicated to the memory of our friend and colleague Chris Armacost.

■ REFERENCES

(1) Kazarinov, R. F.; Suris, R. A. *Fiz. Tekh. Poluprovodn. (S-Peterburg)* **1971**, *5*, 797−800.
(2) Faist, J.; Capasso, F.; Sivco, D. L.; Sirtori, C.; Hutchinson, A. L.; Cho, A. Y. *Science* **1994**, *264*, 553−556.
(3) Curl, R. F.; Capasso, F.; Gmachl, C.; Kosterev, A. a.; McManus, B.; Lewicki, R.; Pusharsky, M.; Wysocki, G.; Tittel, F. K. *Chem. Phys. Lett.* **2010**, *487*, 1−18.
(4) Maulini, R.; Beck, M.; Faist, J.; Gini, E. *Appl. Phys. Lett.* **2004**, *84*, 1659−1661.
(5) Caffey, D.; Radunsky, M. B.; Cook, V.; Weida, M.; Crivello, S.; Buerki, P. R.; Day, T. *Proc. SPIE* **2011**, *7953*, 79531K−79531K-11.
(6) Young, C.; Kim, S.; Luzinova, Y.; Weida, M.; Arnone, D.; Takeuchi, E.; Day, T.; Mizaikoff, B. *Sens. Actuators, B* **2009**, *140*, 24−28.
(7) Kosterev, a. a.; Buerki, P. R.; Dong, L.; Reed, M.; Day, T.; Tittel, F. K. *Appl. Phys. B: Laser Opt.* **2010**, *100*, 173−180.
(8) Brandstetter, M.; Genner, A.; Anic, K.; Lendl, B. *Analyst (Cambridge, U.K.)* **2010**, *135*, 3260−5.
(9) Lu, F.; Belkin, M. a *Opt. Express* **2011**, *19*, 19942−7.
(10) Farahi, R. H.; Passian, a; Tetard, L.; Thundat, T. *J. Phys. D: Appl. Phys.* **2012**, *45*, 125101.
(11) Lewicki, R.; Doty, J. H.; Curl, R. F.; Tittel, F. K.; Wysocki, G. *Proc. Natl. Acad. Sci. U.S.A.* **2009**, *106*, 12587−92.
(12) Hofstetter, D.; Di Francesco, J.; Hvozdara, L.; Herzig, H. P.; Beck, M. *Appl. Phys. B: Laser Opt.* **2011**, *103*, 967−970.
(13) Goddard, A. F.; Logan, R. P. H. *Aliment. Pharmacol. Ther.* **1997**, *11*, 641−649.
(14) Cao, W.; Duan, Y. *Clin. Chem. (Washington, DC, U.S.)* **2006**, *52*, 800−811.
(15) Trimmel, H.; Luschin, U.; Köhrer, K.; Anzur, C.; Vevera, D.; Spittler, A. *Shock* **2012**, *37*, 140−4.
(16) Mizock, B. A. *Best Pract. Res., Clin. Endocrinol. Metab.* **2001**, *15*, 533−551.
(17) Barth, E.; Albuszies, G.; Baumgart, K.; Matejovic, M.; Wachter, U.; Vogt, J.; Radermacher, P.; Calzia, E. *Crit. Care Med.* **2007**, *35*, S508−18.
(18) Rossetti, L.; Giaccari, A.; Barzilai, N.; Howard, K.; Sebel, G.; Hu, M. *J. Clin. Invest.* **1993**, *92*, 1126−1134.
(19) Vary, T. C.; Siegel, J. H.; Nakatani, T.; Sato, T.; Aoyama, H. *JPEN, J. Parenter. Enteral Nutr.* **1986**, *10*, 351−355.
(20) Slater, C.; Preston, T.; Weaver, L. T. *Rapid Commun. Mass Spectrom.* **2001**, *15*, 1270−1273.
(21) Barth, E.; Tugtekin, I.; Weidenbach, H.; Wachter, U.; Vogt, J.; Radermacher, P.; Adler, G.; Georgieff, M. *Isot. Environ. Health Stud.* **1998**, *34*, 209−213.
(22) Amann, A.; Spaněl, P.; Smith, D. *Mini-Rev. Med. Chem.* **2007**, *7*, 115−129.
(23) Cao, W.; Duan, Y. *Crit. Rev. Anal. Chem.* **2007**, *37*, 3−13.
(24) Wong, W. W.; Hachey, D. L.; Zhang, S.; Clarke, L. L. *Rapid Commun. Mass Spectrom.* **1995**, *9*, 1007−1011.
(25) Haisch, M.; Hering, P.; Fuss, W.; Fabinski, W. *Isot. Environ. Health Stud.* **1994**, *30*, 247−251.
(26) Vogt, J. a.; Wachter, U.; Mehring, J.; Radermacher, P.; Georgieff, M.; Fischer, H.; Holscher, U.; Moede, M.; Fabinski, W. *J. Appl. Physiol.* **2009**, *107*, 302−307.
(27) Braden, B.; Gelbmann, C.; Dietrich, C. F.; Caspary, W. F.; Schölmerich, J.; Lock, G. *Eur. J. Gastroenterol. Hepatol.* **2001**, *13*, 807−810.
(28) Van Der Hulst, R. W.; Lamouliatte, H.; Megraud, F.; Pounder, R. E.; Stolte, M.; Vaira, D.; Williams, M.; Tytgat, G. N. *Aliment. Pharmacol. Ther.* **1999**, *13*, 1171−1177.
(29) Murnick, D. E.; Peer, B. J. *Science (Washington, DC, U.S.)* **1994**, *263*, 945−947.
(30) Faist, J.; Gmachl, C.; Capasso, F.; Sirtori, C.; Sivco, D. L.; Baillargeon, J. N.; Cho, A. Y. *Appl. Phys. Lett.* **1997**, *70*, 2670−2672.
(31) Gmachl, C.; Baillargeon, J. N.; Capasso, F.; Sirtori, C.; Sivco, D. L.; Chu, S. N. G.; Cho, A. Y. *IEEE Photonics Technol. Lett.* **1997**, *9*, 1090−1092.
(32) Rubin, T.; von Haimberger, T.; Helmke, A.; Heyne, K. *J. Breath Res.* **2011**, *5*, 027102.
(33) Croitoru, N.; Dror, J.; Goldenberg, E. *Fiber Integr. Opt.* **1987**, *6*, 347−361.
(34) Dahan, R.; Dror, J.; Croitoru, N. *Mater. Res. Bull.* **1992**, *27*, 761−766.
(35) Wilk, A.; Seichter, F.; Kim, S.-S.; Tütüncü, E.; Mizaikoff, B.; Vogt, J. a; Wachter, U.; Radermacher, P. *Anal. Bioanal. Chem.* **2012**, *402*, 397−404.
(36) Kim, S.-S.; Menegazzo, N.; Young, C.; Chan, J.; Carter, C.; Mizaikoff, B. *Appl. Spectrosc.* **2009**, *63*, 68A−86A.
(37) Seichter, F.; Wilk, A.; Wörle, K.; Kim, S.-S.; Vogt, J. A.; Wachter, U.; Radermacher, P.; Mizaikoff, B. *Anal. Bioanal. Chem.* **2012**, accepted for publication.
(38) Wold, S. *Chemom. Intell. Lab. Syst.* **2001**, *58*, 109−130.
(39) de Jong, S. *Chemom. Intell. Lab. Syst.* **1993**, *18*, 251−263.